A cost-effective, modular, research-grade optical microscope

Anupam Bharadwaj[1], Ranjan Kalita[2], Amalesh Kumar[1], Anupam Sarma[3], Bithiah G. Jaganathan[4], Sunil Kumar[5], Frederik Gorlitz[5], Jonathan Lightley[5], Chris Dunsby[5], Mark Neil[5], Callum Hollick[6], Jeremy Graham[6], P. M. W. French[5] and Bosanta R. Boruah[1,*]

[1]Department of Physics, Indian Institute of Technology Guwahati, Guwahati 781 039, India
[2]Department of Physics, Pragjyotish College, Guwahati 781 009, India
[3]Department of Onco-pathology, Dr B. Borooah Cancer Institute, Guwahati 781 016, India
[4]Department of Biosciences and Bioengineering, Indian Institute of Technology Guwahati, Guwahati 781 039, India
[5]Photonics Group, Department of Physics, Imperial College London, London SW7 2AZ, UK
[6]Cairn Research Ltd, Graveney Road, Faversham, Kent ME13 8UP, UK

Optical microscopy is a ubiquitous tool in the physical and life sciences and in histopathology, where visible light microscopy is used to analyse clinical tissue sections at the micron scale to help diagnose diseases. In recent years, microscope technologies have dramatically evolved, but these have generally come with increased cost and complexity. To widen access to advanced microscopy capabilities, we have developed a cost-effective modular platform for optical microscopy (www.openscopes.com). Many of these instruments can be based around a new low-cost and flexible microscope stand, 'openFrame', for which the core components are open source. openFrame can support implementations of a wide range of microscope modalities for diverse applications, including research, pathology and training. Unlike many commercial microscopes that are often designed for specific applications and cannot be easily upgraded or adapted for different imaging modalities, openFrame-based instruments can be relatively easily maintained, upgraded or adapted to another modality without requiring manufacturer support. To this end, openFrame-based instruments are envisaged to operate with open-source software, enabling researchers to assemble and modify their microscopes with minimal challenges presented by proprietary (closed) hardware or software. Here, we describe the implementation of a low-cost, research-grade modular optical microscope applicable to research and pathology.

Keywords: Clinical diagnosis, imaging modalities, modular optical microscope, open-source software, research and pathology.

OPTICAL microscopes are ubiquitous in the physical and biological sciences, typically using visible electromagnetic radiation for diverse imaging applications in the fields of cell biology[1,2], biotechnology[3,4], life sciences[5,6], nanotechnology[7,8], and also in the examination of histopathology tissue sections for clinical diagnosis[9–11]. In recent decades, advances in technology have dramatically expanded the capabilities of optical microscopy, driven in part by the progress in computational techniques, as well as in light sources and detectors. There is wide interest in implementing advanced microscopy techniques, as well as in exploiting standard instruments for biology and medicine. Most workhorse optical microscopes provide a trans-illumination mode for brightfield imaging. Many offer wide-field epi-fluorescence imaging using LED, lamp or laser sources for fluorescence excitation, and scientific cameras (with sufficient sensitivity for single photon detection) are used for detection. A commercial research-grade microscope integrating these modalities typically costs over 5,000,000 Indian rupees (INR), which can limit access for scientists in many situations. The capabilities of such a microscope can, however, be realized at a significantly reduced cost by assembling a modular instrument from off-the-shelf optical, mechanical and electronic components, and using open-source software. For example, high-power solid-state lasers can be replaced with industrial-grade diode lasers, and scientific cameras such as EMCCD or sCMOS cameras can be replaced with CMOS machine vision cameras – and the newly available, lower cost-cooled CMOS cameras (www.cellcam.co.uk/cameras/). Objective lenses with high numerical apertures (e.g. 100× oil immersion, 1.30 NA (Numerical Aperture)) lenses are available at a reasonable cost (<60,000 INR), and personal computers specified for gaming applications are sufficient for most microscopy image processing. However, the main microscope stand can still be expensive, and proprietary hardware and software may present challenges when implementing a new microscopy technique on a commercial microscope frame. In principle, it is possible to assemble an entire microscope from self-fabricated components or from generic optomechanical components, but this requires significant, specific expertise beyond most microscope users.

*For correspondence. (e-mail: brboruah@iitg.ac.in)

Here, we describe the implementation of an optical microscope based on the modular 'openFrame' microscope stand[12] designed to enable non-experts to rapidly configure and assemble research-grade microscopes for a lower component cost than would be required to assemble one entirely from generic commercial optomechanical components. We report the first translation of the openFrame concept from its originating laboratory at Imperial College London, UK[12,13] to a research laboratory in India, demonstrating the broad potential applicability of a modular, self-assembled open microscope to research and clinical pathology. The latest versions of the CAD files for the modules of the basic openFrame-based microscope stand are freely shared[12,14] to enable mechanical workshops to fabricate their components or to get them manufactured locally, or they can be purchased[15].

The basic openFrame stand comprises modular anodized aluminum layers that can house optical components such as mirrors, lenses or dichroic beam splitters along a central optical axis, which can be coupled to optomechanical components and devices such as cameras or lasers. The layers are modules that can be assembled to provide a wide range of configurations, including multiple camera ports or fluorescence excitation ports for LED or laser illumination.

The openFrame-based microscopes can be implemented with a manual translation stage to hold and adjust the focus of a sample, or they can be configured with a motorized module, e.g. utilizing a piezoelectric actuator for axial scanning of the objective lens and a computer-controlled motorized *x*–*y* stage, e.g. to enable multiwell plate imaging or slide scanning. A trans-illumination pillar can be fitted for brightfield illumination using an LED light source. To date, openFrame-based instruments have been applied to fluorescence and quantitative phase imaging[16] and to super-resolved microscopy using the cost-effective easySTORM[17] implementation of direct stochastic optical super-resolution microscopy (dSTORM)[18,19] that exploits multimode diode lasers delivered by multimode optical fibres for excitation. It has also been adapted to carry out automated microscopy for high-content analysis through an open-source optical autofocus module[13,20]. The modular openFrame concept is relatively compact, enabling it to be installed in confined spaces such as incubators or biosafety confinement facilities, making it convenient to transport the instrument. The implementation of an openFrame-based microscope at the Indian Institute of Technology, Guwahati, presented here, utilizes affordable, industry-grade components. We demonstrate its performance in the transillumination and epi-fluorescence modes by imaging a test target, quantum dots (QDs) and clinical histological specimens.

Description of the constituent components and modules of the openFrame-based microscope

Most optical microscopes are configured around core components, including an objective lens, illumination source, sample-stage, eyepiece or camera and microscope stand. To realize this, the openFrame-based fluorescence microscope comprises four modular openFrame layers, a base plate, a sample-stage adapter and a trans-illumination pillar supporting an LED transillumination source (Figure 1). These layers are rigidly clamped together, but their relative orientation can be adjusted in steps of 45° about the optical axis for experimental convenience. Layer 1 is the detection module containing a mirror with its reflecting surface orientated at 45° to the vertical optical axis to direct image-bearing light to a camera that can be mounted on the side of the layer 1. Layer 2 is a 'tube lens' module, and layer 3 contains the filter cube that introduces the excitation radiation into this fluorescence microscope. Layer 4 supports a mounting for the microscope objective centred on the openFrame optical axis. This mounting includes a piezoelectric actuator (Physik Instrumente, Q.545 used with E-873 controller) that translates the microscope objective axially, i.e. along the vertical *Z*-direction. A sample-stage adapter layer is mounted on top of the (objective lens) layer 4, onto which a motorized *X*–*Y* microscope stage is mounted. A transillumination pillar is also fixed at one of the edges of the stage-adapter layer. This system is computer-controlled using the open-source μManager program[21], and enables imaging in the transillumination or epi-fluorescence modes. Below, we provide details of the specific components used in the openFrame-based microscope, along with a rendering of the CAD representation of the openFrame modular stand.

Transillumination for brightfield imaging

The transillumination pillar, as seen in Figure 1, is an inverted, *L*-shaped stand with an LED source (MONOLED, Cairn Research Ltd, UK), along with a condenser lens of NA = 0.34, attached to its horizontal arm. The pillar is fixed to the *X*–*Y* stage adapter. The horizontal arm of the pillar can be translated vertically to adjust the illumination at the sample plane. The light transmitted through the sample in transillumination mode is detected by a camera mounted on layer 1 after passing through layers 4 → 2 and being reflected at the 45° mirror in layer 1.

X–Y microscope sample stage

A motorized *X*–*Y* stage (ASR100B120B-E03T3A, Zaber, Canada) is installed on the stage-adapter layer that is bolted onto layer 4. The *X*–*Y* stage can be controlled via a PC running the hardware–software integration (X-MCB2-KX14BG controller, Zaber Console software). It is also possible to control the stage with a joystick (X-JOY3-PTB2, Zaber).

Objective lens focusing

Layer 4 contains the objective lens, which is mounted on an *L*-bracket to be centred on the vertical openFrame optical

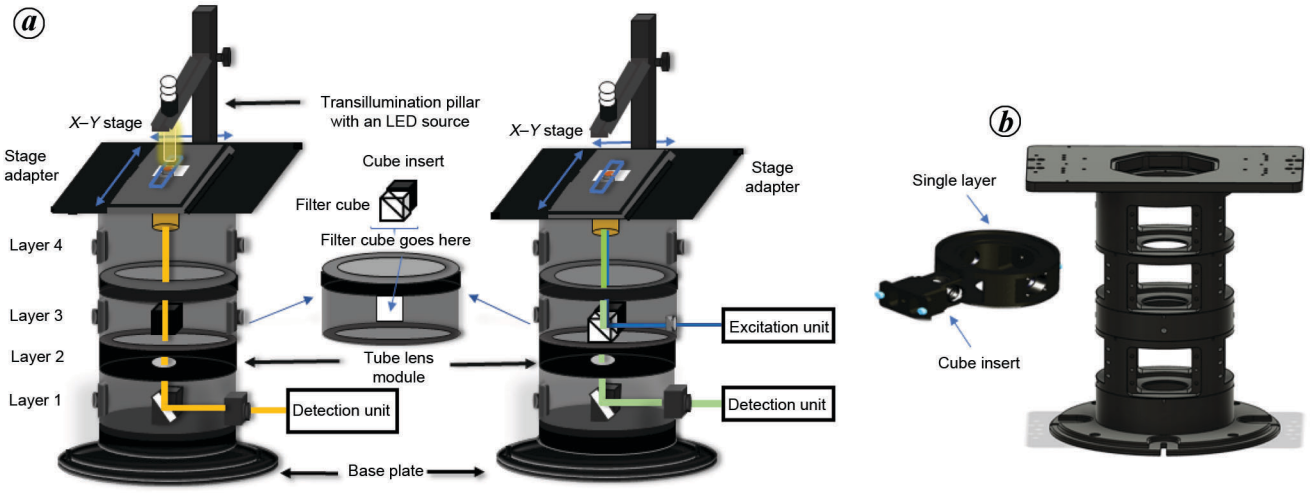

Figure 1. ***a***, Schematic of the openFrame-based microscope showing the four layers, viz. base plate, *X*–*Y* sample stage, trans-illumination pillar and other hardware components. ***b***, CAD representation of the openFrame modular microscope stand and a single layer with the cube insert.

axis. To adjust the focusing of the microscope, the objective lens bracket is fitted to a linear precision piezoelectric stage with an encoder providing 1 nm resolution (Q-545.140, Physik Instrumente). The stage controller (E-873 PI Shift Controller, Physik Instrumente) is programmed using the software PI MikroMove controlled by µManager. We have used three microscope objective lenses: PLN 20× 0.40 NA (Olympus Optical), PlanF 40× 0.75 NA, (AmScope) and PlanF 100× oil immersion 1.3 NA (AmScope). This openFrame layer can also accommodate a dichroic beam splitter that can be used to introduce an infrared laser beam for an optional autofocus module or to implement other functionalities[13].

Fluorescence excitation

Layer 3 houses the excitation filter cube and has side ports onto which the optical systems for coupling in the excitation light can be mounted. In this implementation, layer 3 has a mechanical slider that can accommodate two filter cubes containing dichroic beam-splitters that reflect the radiation entering from the side port up through the objective lens to the sample and transmit the fluorescence emission down towards layer 1 and the camera. Each filter cube contains excitation, dichroic and emission filters. Typically, we use a multiline dichroic filter that enables multiple fluorescence excitation wavelengths to be utilized. If one cube position is left empty, then the mechanical slider can be set to allow the transmitted light to pass through layer 1 to the camera for brightfield imaging. Alternatively, in place of a mechanical slider, a single filter cube can be mounted (Figure 1 *a* and *b*), which needs to be removed to allow transmitted light to pass through for brightfield imaging. The filter cube holder accommodates a 25.5 × 36 mm dichroic mirror and 25 mm diameter excitation and emission filters. These commonly used sizes allow for the convenient changing of the optical filters with other microscopes according to experimental requirements.

The filter cube used here in layer 3 contains a bespoke multi-line dichroic beam-splitter (ZT405/462/635/830rpc-UF2, (lot-339819 Chroma technology)) with matching emission filter (ZET405/462/635/830m, (lot-339636 Chroma technology)), and can be used with an excitation filter (ZET405/465/625/825x; Chroma technology). Alternatively, individual band-pass excitation filters can be used. This specific dichroic beam-splitter and emission filter combination is designed to work with single or multiwavelength excitation at 405, 462 and 635 nm, and transmit emission within bands at 408–457, 472–627 and 645–820 nm. The dichroic beam-splitter also reflects radiation above 820 nm, which can be used for an optical autofocus system[13].

To provide excitation radiation for fluorescence microscopy, we assembled a computer-controlled laser bank of multimode diode lasers to provide switchable excitation at multiple wavelengths (Figure 2). The laser bank includes four multimode diode laser modules (LDM-638-700-C, LDM-520-1000-C, LDM-462-1400-C and LDM-405-350-C; Lasertack GmbH), labelled DL1–DL4, providing multimode continuous wave laser radiation centred on wavelengths of 638, 520, 462 and 405 nm with maximum power of ~700, ~1000, ~1400 and ~350 mW respectively. To block amplified spontaneous emission and ensure narrowband excitation, e.g. for use with our multiline dichroic beam splitter and emission filter, we use four bandpass filters (#65106, #65093, #39308 and #65072; Edmund Optics), labelled as BP 1–BP 4, each of 10 nm FWHM (full width at half maximum) and place them in front of the respective diode laser module outputs. A suitable combination of three dichroic beam combiners, labelled as DBC1, DBC2 and DBC3 (#86394, #86324 and #86389, Edmund Optics), and nine broadband dielectric mirrors (M1–M9, BB05-E02, Thorlabs) mounted in kinematic mounts steer

the laser beams from the four diode lasers to be collinear at the lens L4, which focuses the laser radiation into a multimode optical fibre. The diode laser drivers, LD1–LD4 (2.5 A iLD driver, Lasertrack GmBH), provide linear control of the laser powers through a steady control current that is regulated by modulating the driver voltages using four programable Arduino microcontrollers[21,22], AD1–AD4, each with an associated analogue to digital converter (ADC; TLV5618AI, Texas Instruments). Each driver also provides temperature control through an integral thermoelectric cooler (TEC) driver, as well as an interlock mechanism. The µManager program controlling the microscope can address these Arduino microcontrollers to control the fluorescence excitation. The components for this laser bank cost approximately 500,000 INR.

Tube lens

Layer 2 in the openFrame stack houses a tube lens of 200 mm focal length (#58-520, Nikon), which relays the fluorescence or transmitted light from the objective lens to the camera.

Detection

Layer 1 generally incorporates a silver-coated right-angled mirror (#89-632, Edmund Optics) mounted on the optical axis of the openFrame that reflects the incident light to a camera mounted on the side port of the layer. This unit houses two such mirrors on a mechanical slider that can be switched to direct the incident light to cameras mounted on ports on opposite sides of the layer. In the present configuration, we use only one such port that detects light from the sample after being reflected from the right-angled mirror.

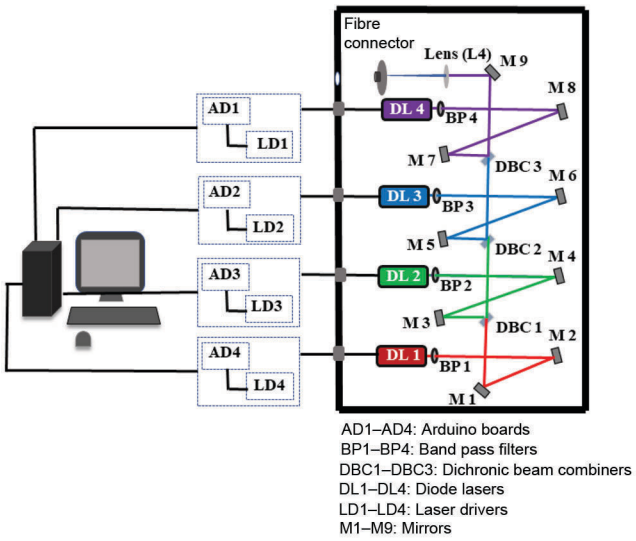

Figure 2. Schematic of the PC-controlled laser bank equipped with lasers, optics and electrical components which are a part of the excitation unit.

We use two low-cost, fan-cooled CMOS cameras: a monochrome camera (CellCam Centro 200MR, Cairn Research Ltd) primarily used for fluorescence imaging and a colour CMOS camera (CellCam Rana 200CR, Cairn Research Ltd) primarily used for brightfield imaging with white-light transillumination. Both cameras use the Sony IMX 183 CMOS sensor, which has a 5440 × 3648 array of 2.4 µm pixels, although the colour filter mask on the colour CMOS camera effectively reduces the number of pixels by 4.

Software

To control all the components of this brightfield cum fluorescence microscope using a personal computer interface, we use µManager[21–24], a Java-based open-source software tool for light microscopy that has a comprehensive list of device adapter software for various instrument/hardware components. Many commercial hardware components are supplied with a DLL (dynamic library link). Once the respective DLL file is installed, µManager provides the option to configure and control the hardware through its software control panel using the relevant device adapter software. For our system, the µManager is configured to control the *X*–*Y* stage and the *Z*-drive, image acquisition by the two cameras and modulation of the output power of the four excitation lasers. It also has options to configure and control the LED sources[25–27]. For image analysis, µManager can be used with the open-source software ImageJ[28], for which further functionality is available, as demonstrated by the open-source software FIJI[29].

Implementation of the openFrame-based microscope

Figure 3 depicts the complete openFrame-based optical microscope configuration used here. This schematic indicates how light from the diode lasers inside the laser bank is delivered to the excitation unit mounted on openFrame layer 3 through a multimode optical fibre (MMF) cable. The excitation unit comprises a fibre connector (SM1-FC/PC, Thorlabs) attached to a lens tube (SM105, Thorlabs) that contains lens L2, which collimates the excitation radiation emerging from MMF and directs it to lens L1, which focuses it to the back focal plane of the microscope objective lens. MMF is vibrated to mix the spatial modes of the radiation and cause any speckles formed in the illuminated area of the sample plane to be time-averaged to provide spatially uniform illumination. This uniform illumination is provided over ~125, 315 and 630 µm diameter circular fields of view, using the 100×, 40× and 20× microscope objective lenses respectively. The illuminated area of the sample plane depends on the NA of MMF. In this case, the NA of MMF with a 50 µm core (FG050UGA-CUSTOM, Thorlabs) is 0.22. This arrangement can deliver up to 90% of the laser power to the objective back aperture.

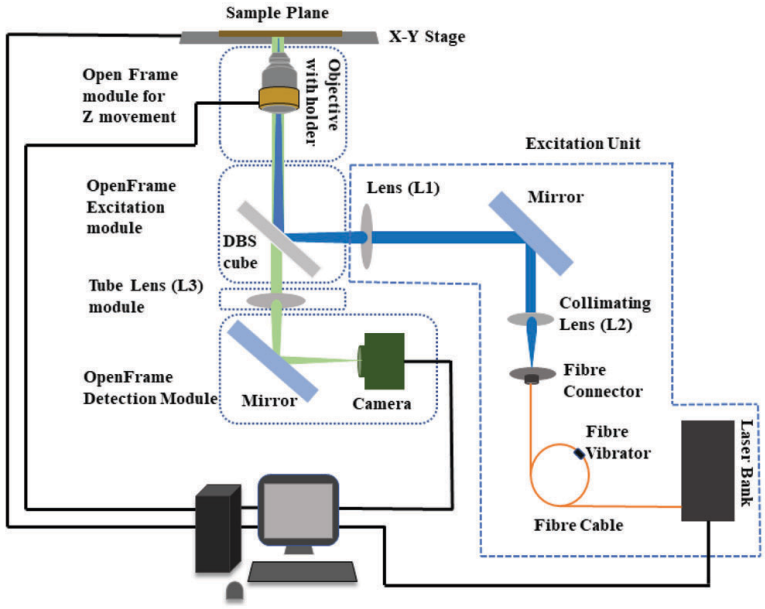

Figure 3. Schematic of the complete openFrame-based microscope implemented by assembling the necessary hardware, optical, opto-electronic and electronic components.

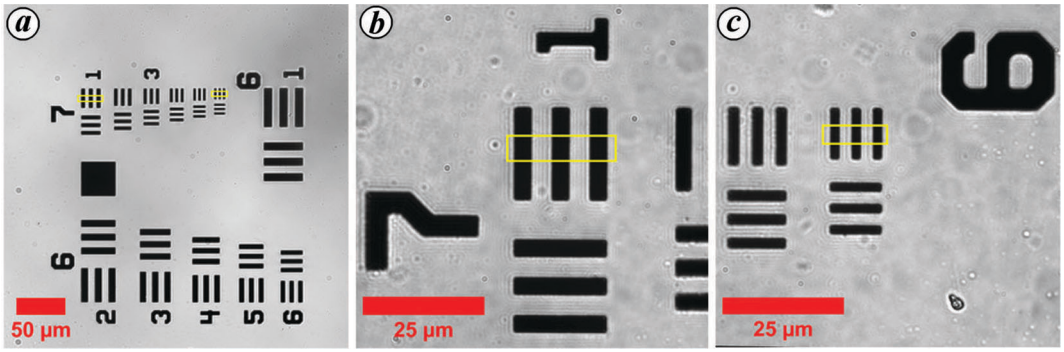

Figure 4. Trans-illumination images of a 1951 USAF test target with (***a***) 20× objective lens, (***b***) 100× objective lens showing the G7E1 pattern and (***c***) 100× objective lens showing the G7E6 pattern captured by the monochrome camera. The yellow rectangles indicate the directions in which line profiles are drawn for estimating the width of the respective strips.

Results and discussion

Brightfield imaging using transmitted light

To demonstrate the openFrame-based microscope in the transillumination mode, we imaged a positive 1951 USAF test target (R3L3S1P, Thorlabs). The image acquisition was controlled using µManager, and the captured images were analysed in FIJI. Figure 4 *a* shows the image of the test target using the 20× objective lens, while Figure 4 *b* and *c* show the image of the same target using the 100× objective lens with immersion oil. The target comprises a number of patterns of opaque strips, including the patterns for group 7, element 1 (G7E1) and G7E6, indicated as regions of interest (ROIs) by yellow rectangles. We plotted the grey-scale intensity profiles against the pixel number along a line normal to the strips, and from each line profile, we calculated the FWHM of the opaque and transparent strips inside the particular ROI. We then compared the estimated values with the corresponding widths specified by the manufacturer. Table 1 shows that the measured mean FWHM values of the strips are in reasonable agreement with those in the supplied specification, confirming that the microscope and camera are reasonably well-configured.

Imaging using the epi-fluorescence mode (multiwavelength excitation)

To demonstrate the epi-fluorescence mode of the openFrame-based microscope with multiwavelength excitation, we imaged a mixture of crimson red (F8806 FluoSpheres® carboxylate, Invitrogen™) fluorescence beads of particle

Table 1. Measured width of a strip in the G7E1 and G7E6 patterns of the 1951 USAF resolution test chart using different objective lenses in the trans-illumination mode

Pattern	Specified width of a black strip (µm)	Measured width of a black strip with different objective lenses (µm)	
		20 × 0.4 NA	100 × oil immersion 1.3 NA
G7E1	3.91	3.99	3.92
G7E6	2.19	2.31	2.2

NA, Numerical Aperture.

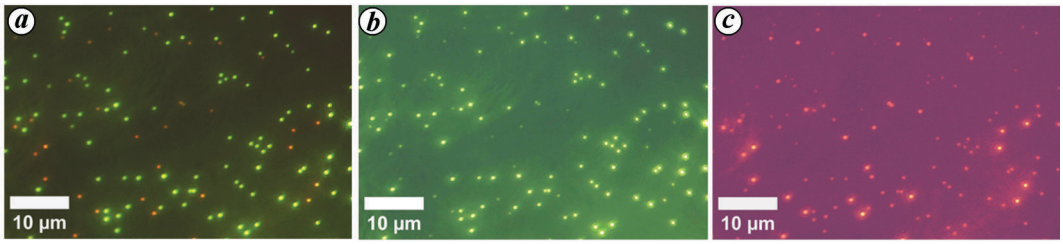

Figure 5. Epi-fluorescence images of the specimen slide containing a mixture of crimson red and orange–green fluorescent beads, excited with (***a***) both 462 and 638 nm lasers, using the 100× objective lens on the colour CMOS camera, (***b***) 462 nm laser and (***c***) 638 nm laser.

size 220 nm and orange–green (F8809 FluoSpheres® carboxylate, Invitrogen™) fluorescence beads of particle size 200 nm, diluted in deionized water and kept between a cover glass and a microscope glass slide. The crimson red beads can be predominantly excited using the 638 nm laser, while the orange–green beads can be predominantly excited using the 462 nm laser. We first used the 100× objective lens and the fluorescence filter cube in layer 3 to image the specimen slide excited with the 638 and 462 nm diode lasers when switched on simultaneously and recorded the image using the colour (CellCam Rana 200CR colour CMOS) camera (Figure 5 *a*). The multi-line dichroic beam splitter and filter set allow fluorescence light from the beads excited by both 638 and 462 nm radiation to be imaged simultaneously. We then exited the same region on the slide using the 462 nm diode laser. Figure 5 *b* shows the image of the respective beads. We then switched on the 638 nm diode laser, and Figure 5 *c* shows the image of the respective beads. Figure 5 shows this multispectral epi-fluorescence modality of the openFrame-based microscope using dual excitation wavelengths, showing both the crimson red beads with orange and orange–green beads with light green colour.

Comparison with a standard commercial microscope for the brightfield and epi-fluorescence modes

We compared the performance of the openFrame-based microscope with a standard commercial fluorescence microscope (IX51, Olympus) in the epi-fluorescence mode by imaging carboxyl QDs (Q21361MP, Invitrogen™) that were diluted in deionized water, and mounted between a microscope glass slide and a cover glass. In both microscopes, we excited the QDs with the 462 nm wavelength laser and used the same monochrome CMOS camera and filter set to record fluorescence images detected in the wavelength range 650–850 nm. These QDs have diameters ranging between 15 and 20 nm, i.e. much smaller than the excitation or emission wavelengths, and hence, their image can directly provide the lateral PSF of the respective microscope[30]. For each fluorescence microscope, we imaged the QDs using a research-grade 100× oil immersion objective lens (UPlanSApo, 1.40 NA, Olympus; cost of ~400,000 INR) and a cheaper (cost of ~60,000 INR) 100× oil immersion lens (Plan Fluor PF100X-INF, 1.3 NA, AmScope).

We first imaged the QDs with the Olympus IX51 microscope using the Olympus 1.4 NA objective lens and then imaged another area of the QD slide with the AmScope 1.3 NA objective lens (Figure 6 *a* and *b* respectively). We then imaged different areas of the QD slides using the same two objective lenses in the openFrame-based microscope (Figure 6 *c* and *d* respectively). From each image in Figure 6, we selected a random set of isolated QDs and plotted intensity versus position through the centre of the images of the isolated QDs. Figure 6 *e–h* shows the raw and Gaussian fitted-line plots for a particular isolated QD taken from Figure 6 *a–d* respectively. The mean FWHM of the line plot for each image measures the experimental lateral point spread function (PSF). The lateral FWHM of the theoretical diffraction-limited PSF was 0.51 λ/NA (ref. 31). Table 2 presents a comparison of the mean lateral FWHM values of the experimental PSFs of eight QDs in each case and theoretical prediction for the two objective lenses.

The table shows that the experimentally obtained lateral PSF is not significantly different when measured on either

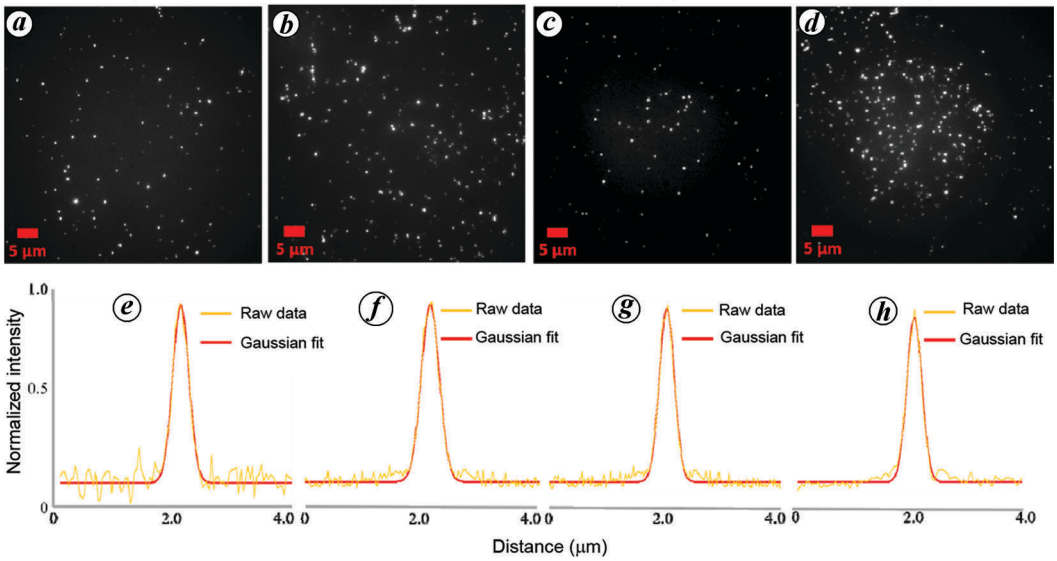

Figure 6. ***a***, ***b***, Epi-fluorescence images of quantum dots (QDs) on the monochrome CMOS camera obtained using the commercial (Olympus IX51) fluorescence microscope with (***a***) 1.4 NA Olympus and (***b***) 1.3 NA AmScope objective lenses respectively. ***c***, ***d***, Images of QDs acquired using the same monochrome CMOS camera obtained in the epi-fluorescence mode using the openFrame-based microscope with the same (***c***) 1.4 NA Olympus and (***d***) 1.3 NA AmScope objective lenses respectively. ***e***–***h***, Plots of raw intensity data and the respective fitted line plots for an isolated QD chosen randomly from images ***a***–***d*** respectively.

Table 2. Theoretically and experimentally obtained full width at half maximum (FWHM) of lateral PSF for the standard optical microscope and the openFrame-based microscope using the same two objective lenses

		FWHM of lateral PSF (theory) using λ = 705 nm		Mean FWHM of lateral PSF measured using CMOS camera (with 2.4 µm pixel size corresponding to 24 nm in the sample plane)			
				Standard commercial microscope		openFrame-based microscope	
Quantum dot (QD) type	QD size	1.4 NA 100× objective lens	1.3 NA 100× objective lens	1.4 NA 100× Olympus lens	1.3 NA 100× AmScope lens	1.4 NA 100× Olympus lens	1.3 NA 100× AmScope lens
Carboxyl QDs peak emission at 705 nm	15–20 nm	256 nm	276 nm	310 ± 3 nm	328 ± 2 nm	311 ± 4 nm	324 ± 3 nm

microscope using the same excitation wavelength, camera, filter set and objective lens, and that using the low-cost 1.3 NA AmScope objective lens provides a resolution only ~5% worse than that obtained using the more expensive 1.4 NA Olympus objective lens. Note that, in general, the lateral FWHM of a lens with 1.3 NA should theoretically be ~7.7% wider than that of a lens with 1.4 NA. Table 2 shows that the openFrame-based microscope with a low-cost objective lens provides comparable image quality with a commercial microscope using the same objective lens, and that the openFrame-based and commercial (Olympus) microscopes also provide similar lateral FWHM when using the same (Olympus) objective lens of the same numerical aperture. We then imaged a specimen slide of unstained human glioblastoma cells (U87MG) using both the brightfield and epi-fluorescence modes to compare the images acquired using the openFrame-based microscope and the commercial optical microscope (IX51, Olympus). Here we used a PlanF 40X 0.75 NA, (PF40X-INF, AmScope) lens in the openFrame-based microscope and a 40×, 0.60 NA (LUCPlanFLN, Olympus Optical) lens in the Olympus IX51 microscope while using the same colour CMOS camera and filter cube in both systems. Figure 7 *a* and *c* show the brightfield image of two different areas from the specimen, obtained using the Olympus microscope in the transillumination mode. Figure 7 *e* and *g* show the brightfield images of the same area respectively, when imaged with the openFrame-based microscope without any filter cube. We further studied the autofluorescence by exciting the same area on the specimen slide with a 462 nm diode laser, and imaging in the epi-fluorescence mode using both the Olympus IX51 microscope and the openFrame-based microscope. Figure 7 *b* and *d* show the recorded autofluorescence image using the Olympus IX51 microscope, while Figure 7 *f* and *h* show the acquired using the openFrame-based microscope. We see that the cells autofluoresce in the light-yellowish range with the 462 nm laser excitation in the epi-fluorescence mode. Figure 7 demonstrates that the performance of the openFrame-based microscope is similar to that of the Olympus IX51 fluorescence microscope.

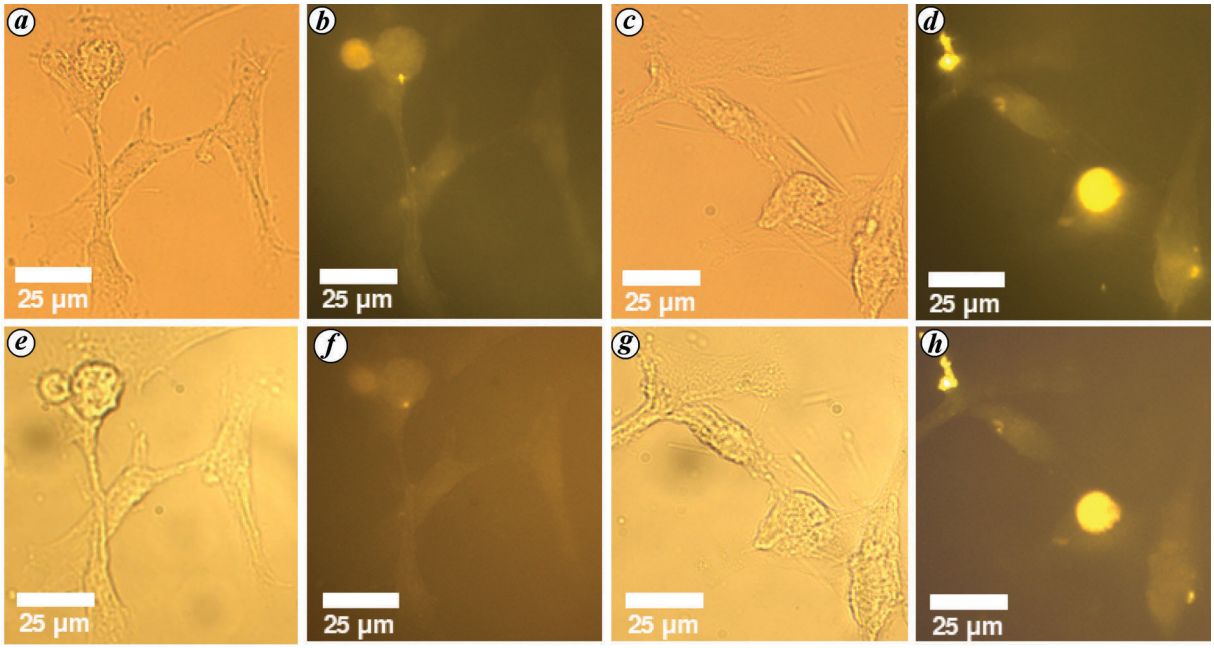

Figure 7. (***a***, ***c***) Brightfield and (***b***, ***d***) fluorescence images of two areas on the specimen slide of unstained human glioblastoma cells (U87 MG) acquired on Olympus IX51 microscope with 40×, 0.60 NA objective lens (LUCPlanFLN, Olympus). (***e***, ***g***) Brightfield and (***f***, ***h***) fluorescence images of the same fields of view acquired subsequently on the openFrame-based microscope with a low-cost 40× 0.75 NA objective lens (PF40X-INF, AmScope). The brightfield images were acquired using the colour CMOS (CellCam Rana 200CR) camera, while fluorescence was excited at 462 nm and acquired using the same colour CMOS camera.

The fluorescence images acquired on the openFrame-based microscope are expected to be dimmer because the fluorophores in the field of view would already have undergone photobleaching during fluorescence image acquisition on the Olympus microscope.

Clinical application (histopathological analysis)

We explored the use of the openFrame-based microscope in the transillumination and epi-fluorescence modes for clinical application by imaging specimen slides of human breast tissue sections stained with hematoxylin and eosin (H&E) to detect normal and cancerous regions[32,33]. Figure 8 *a* shows the transillumination image of normal ducts, while Figure 8 *b* shows cancerous ducts from human breast tissue sections imaged using a standard optical microscope in the Department of Pathology at Dr B. Borooah Cancer Institute, Guwahati (based on an Eclipse 50i, NIKON) with a 40× objective lens (Nikon Plan, 40X/0.65 NA). In Figure 8 *a,* the normal ducts present elliptical rings of epithelial cells inside them, while the image of the cancerous duct in Figure 8 *b* shows infiltration into nearby ducts and the cytoplasmic regions. Further, regular rings of the epithelial cells are distorted, and many tumour cells appear inside the duct. The same H&E-stained normal and cancerous human breast tissue sections were then imaged using the openFrame-based microscope, using the transillumination mode with the 20× objective lens (Olympus PLN 20X/0.40 NA) and the colour CMOS camera (without the filter cube).

Figure 8 *c* shows the transillumination H&E image of a normal duct (inside the dashed circle), while Figure 8 *d* shows the transillumination H&E image of a cancerous duct (indicated by the dashed circle). As seen in Figure 8 *a*, the image of the normal duct in Figure 8 *c* shows an elliptical ring of epithelial cells. On the other hand, the duct seen in Figure 8 *d* is full of tumour cells and no regular rings of epithelial cells are seen.

The epi-fluorescence images in Figure 8 *e* and *f* correspond to the same fields of view as in Figure 8 *c* and *d* and are excited using the 462 nm laser (with the customized multiline beam-splitter and the matching emission filter inside the filter cube in layer 3). Comparing the epi-fluorescence images with their respective transillumination images, it is clear that the stained cells in the cytoplasmic region, as well as inside the duct, fluoresce in green, while there is no fluorescence from the lumen region. This provides a sharp contrast to the boundary of the normal duct against the surrounding regions. As reported previously[34,35], we note that the green emission is a characteristic of the eosin dye, while hematoxylin shows significant absorbance in the UV–Vis region with negligible emission in this range. The epi-fluorescence image in Figure 8 *f* shows that in the case of a cancerous duct, its boundary is indicated by a dark ring.

Another optical method considered useful for clinical diagnosis is optical coherence tomography (OCT)[36], which can provide three-dimensional volume information of tissue and is being explored for different applications, including the generation of H&E-like images of fresh tissue[37].

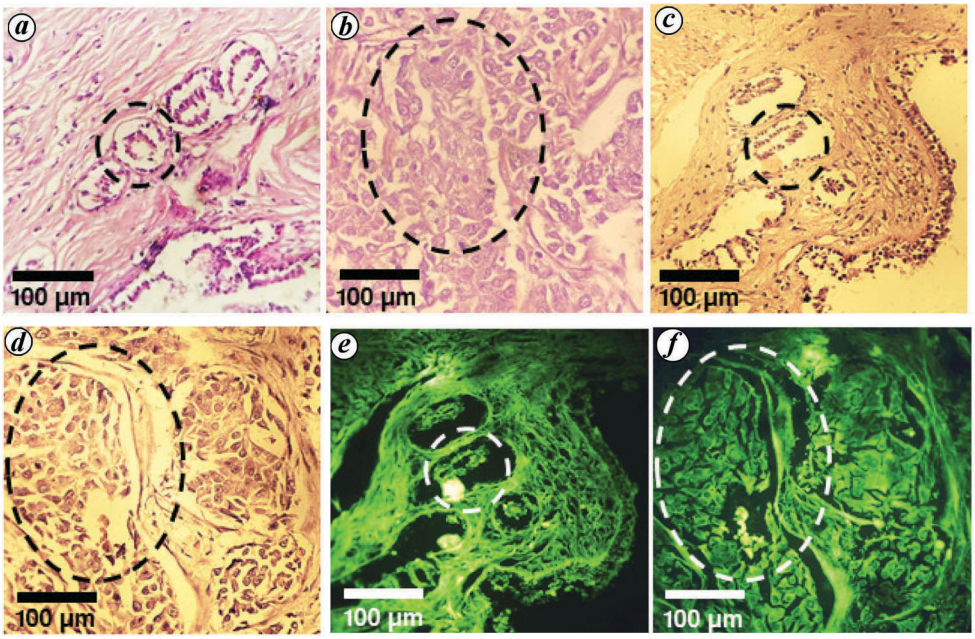

Figure 8. Trans-illumination brightfield images of H&E-stained (***a***) normal and (***b***) cancerous human breast tissue sections under a commercial (Eclipse 50i, NIKON) microscope with a 40× objective lens acquired with a colour CMOS (CellCam Rana 200CR) camera. Trans-illumination brightfield images of H&E-stained (***c***) normal and (***d***) cancerous human breast tissue sections under openFrame-based microscope with 20× objective lens acquired with the same colour CMOS camera. ***e***, ***f***, Epi-fluorescence images, corresponding to (***c***) and (***d***) respectively, using 462 nm excitation laser.

Full-field OCT (FF-OCT) techniques can be implemented on any optical microscope, including the openFrame-based instrument presented here, if suitably adapted. Recently, Liu *et al.*[38] presented an implementation of FF-OCT on an openFrame-based microscope.

Component costs of the openFrame-based microscope

In Table 3, we list the key components necessary to make the modular openFrame-based microscope and estimate their total price (INR). Note that these price estimates were made in 2020, before the COVID-19 pandemic. This list includes the motorized *X*–*Y* stage and the joystick, which cost nearly 700,000 INR. In addition, we have included the price of two CMOS cameras (approx. 100,000 INR per item), the 100× oil immersion objective lens (approx. 60,000 INR), and the dichroic beam splitter and emission filters (approx. 80,000 INR) for epi-fluorescence microscopy. However, instead of the motorized *X*–*Y* stage, one may also use a manual *X*–*Y* stage (e.g. manual Olympus *X*–*Y* Stage, CS S2001, Thorlabs). One could also image with a single camera.

Summary

We have presented the implementation of a cost-effective, modular, research-grade optical microscope on an openFrame-based microscope stand. We have described the key components of the openFrame-based microscope: its main body made of anodized aluminium, including the base, four modular layers accommodating the objective lens, scanning stage, fluorescence filter cube, tube lens and camera-turning mirror, a transillumination pillar and the excitation laser bank. The modular nature and low cost of components, combined with the use of open-source software, facilitate straightforward and affordable maintenance of the entire microscope.

We have shown the ability to operate this openFrame-based microscope in the transillumination mode using an LED transillumination source or in the epi-fluorescence mode using two different excitation lasers. We have demonstrated the research-grade imaging performance of the openFrame-based microscope and have indicated its potential for clinical, histopathological analysis through application to human breast tissue sections. The modular form of openFrame-based microscope makes it easily adaptable to other modalities. While, here we have only implemented conventional brightfield and epifluorescence microscopy, the same could be configured as a super-resolving microscope using easySTORM[13,17], or adapted to quantitative phase microscopy[16]. This open approach to microscope hardware and software enables systems to be assembled and maintained locally in a wide range of laboratory settings, which could widen access to optical microscopy. The openFrame-based microscope in the transillumination mode can be easily converted to a phase-contrast microscope by

Table 3. Rough estimate of the price of the components used in the openFrame-based microscope

Components	Approximate price (Indian rupees)
Excitation and camera port components 1.3 NA oil immersion 100× objective	200,000
Despeckler and power supply	1,250,000
Transillumination pillar and LED source	
PI piezo stage with controller	
CellCam 200MR	
CellCam 200CR	
Zaber motorized *X–Y* stage with controller	
openFrame modular stand	300,000
405 nm diode laser (with laser driver)	134,000
462 nm diode laser (with laser driver)	
520 nm diode laser (with laser driver)	
638 nm diode laser (with laser driver)	
Electronics and metal boxes for diode laser control	280,000
Mirrors, DBC and optical filters	
Mounts, posts, screw and other components inside the laser bank	
Total (gross) price	2,164,000

incorporating an annular mask below the LED source and in the back focal plane of the condenser lens, and using a phase contrast objective lens in layer 4. Alternatively, we can insert a quadrant polarizer mask in the back focal plane of the condenser lens and capture an image of the sample with a polarization-resolving camera to reconstruct quantitative phase images of the sample after appropriate post-processing of the four polarization-resolved images extracted from the captured image, as already demonstrated in an openFrame-based microscope[16]. The performance of any optical microscope can be limited by optical aberrations, including openFrame-based microscopes. The modular flexibility of the openFrame enables an adaptive optics system to be implemented; for example, to compensate for specimen-induced aberrations. It would also be possible to replace the right-angled mirror in layer 1 with a deformable mirror to implement a sensor-less genetic algorithm-based adaptive optics system[39].

Conflict of interest statement: The openFrame concept originated at Imperial College London, UK, and has been co-developed with Cairn Research Ltd (and sister company, Cairn GmbH). An openFrame-based microscope similar to that reported in this study can be made using components fabricated according to CAD files available at https://www.imperial.ac.uk/photonics/research/biophotonics/instruments--software/fluorescence-microscopy/openframe/, or these components can be purchased from Cairn Research Ltd for users who wish to assemble their instruments, but not to fabricate the components themselves. Cairn also designs and sells bespoke application-orientated openFrame-based instruments combining open-source components with proprietary Cairn and third-party components.

1. Sampedro, A. and Howard, V., Cell biological applications of confocal microscopy. *J. Microsc.*, 1994, **175**, 91–92.
2. Jacquemet, G., Carisey, A. F., Hamidi, H., Henriques, R. and Leterrier, C., The cell biologist's guide to super-resolution microscopy. *J. Cell Sci.*, 2020, **133**(11).
3. Halbhuber, K.-J. and König, K., Modern laser scanning microscopy in biology, biotechnology and medicine. *Ann. Anat. – Anat. Anzeiger*, 2003, **185**, 1–20.
4. Wollman, A. J. M., Muchová, K., Chromiková, Z., Wilkinson, A. J., Barák, I. and Leake, M. C., Single-molecule optical microscopy of protein dynamics and computational analysis of images to determine cell structure development in differentiating *Bacillus subtilis*. *Comput. Struct. Biotechnol. J.*, 2020, **18**, 1474–1486.
5. König, K., Multiphoton microscopy in life sciences. *J. Microsc.*, 2000, **200**, 83–104.
6. Borst, J. W. and Visser, A. J. W. G., Fluorescence lifetime imaging microscopy in life sciences. *Meas. Sci. Technol.*, 2010, **21**, 102002.
7. Yao, N. and Wang, Z. L., *Handbook of Microscopy for Nanotechnology*, Kluwer Academic Publishers, New York, 2005.
8. Johnson, S. A., Nanoscopy for nanoscience: how super-resolution microscopy extends imaging for nanotechnology. *WIREs Nanomed. Nanobiotechnol.*, 2015, **7**, 266–281.
9. Poola, P. K., Afzal, M. I., Yoo, Y., Kim, K. H. and Chung, E., Light sheet microscopy for histopathology applications. *Biomed. Eng. Lett.*, 2019, **9**, 279–291.
10. U, A. D. and Mazumder, N., Types of advanced optical microscopy techniques for breast cancer research: a review. *Lasers Med. Sci.*, 2018, **33**, 1849–1858.
11. Garcia, E. *et al.*, Application of direct stochastic optical reconstruction microscopy (dSTORM) to the histological analysis of human glomerular disease. *J. Pathol. Clin. Res.*, 2021, **7**, 438–445.
12. https://www.imperial.ac.uk/photonics/research/biophotonics/instruments--software/fluorescence-microscopy/openframe/ (accessed on 2 June 2023).
13. Lightley, J. *et al.*, openFrame: a modular, sustainable, open microscopy platform with single-shot, dual-axis optical autofocus module providing high precision and long range of operation. *J. Microsc.*, 2023; https://doi.org/10.1111/jmi.13219.
14. https://github.com/ImperialCollegeLondon/openFrame (accessed on 2 June 2023).
15. openFrame components can be purchased from Cairn Research Ltd, https://www.cairn-research.co.uk/product/openframe-microscope/ (accessed on 2 June 2023).
16. Kalita, R. *et al.*, Single-shot phase contrast microscopy using polarisation-resolved differential phase contrast. *J. Biophoton.*, 2021, **14**, e202100144.

17. Kwakwa, K. *et al.*, easySTORM: a robust, lower-cost approach to localisation and TIRF microscopy. *J. Biophoton.*, 2016, **9**, 948–957.
18. Rust, M. J., Bates, M. and Zhuang, X., Sub-diffraction-limit imaging by stochastic optical reconstruction microscopy (STORM). *Nat. Method.*, 2006, **3**, 793–796.
19. Heilemann, M. *et al.*, Subdiffraction-resolution fluorescence imaging with conventional fluorescent probes. *Angew. Chemie Int. Ed.*, 2008, **47**, 6172–6176.
20. Lightley, J. *et al.*, Robust deep learning optical autofocus system applied to automated multiwell plate single molecule localization microscopy. *J. Microsc.*, 2022, **288**, 130–141.
21. Edelstein, A. D., Amodaj, N., Hoover, K., Vale, R. D. and Stuurman, N., Computer control of microscopes using *μManager*. *Curr. Protoc. Mol. Biol.*, 2010, **92**, 14–20.
22. https://www.arduino.cc/ (accessed on 2 June 2023).
23. Stuurman, N., Adapter for the Arduino electronics prototyping platform.
24. Edelstein, A. D., Tsuchida, M. A., Amodaj, N., Pinkard, H., Vale, R. D. and Stuurman, N., Advanced methods of microscope control using *μManager* software. *J. Biol. Methods*, 2014, **1**(2).
25. https://www.cairn-research.co.uk/product/89-north-ldi-support-in-micromanager-test/ (accessed on 4 June 2023).
26. https://www.coolled.com/wp-content/uploads/2014/04/MicroManager-Software-Summary-Sheet-R3.pdf (accessed on 4 June 2023).
27. https://www.thorlabs.com/newgrouppage9.cfm?objectgroup_id=3832 (accessed on 4 June 2023).
28. Schneider, C. A., Rasband, W. S. and Eliceiri, K. W., NIH Image to ImageJ: 25 years of image analysis. *Nat. Method.*, 2012, **9**, 671–675.
29. Schindelin, J. *et al*., Fiji: an open-source platform for biological-image analysis. *Nat. Method.*, 2012, **9**, 676–682.
30. Yoo, H., Song, I. and Gweon, D.-G., Measurement and restoration of the point spread function of fluorescence confocal microscopy. *J. Microsc.*, 2006, **221**, 172–176.
31. Wilson, T., Resolution and optical sectioning in the confocal microscope. *J. Microsc.*, 2011, **244**, 113–121.
32. Alturkistani, H. A., Tashkandi, F. M. and Mohammedsaleh, Z. M., Histological stains: a literature review and case study. *Global J. Health Sci.*, 2015, **8**, 72.
33. Fischer, A. H., Jacobson, K. A., Rose, J. and Zeller, R., Hematoxylin and eosin staining of tissue and cell sections. *Cold Spring Harb. Protoc.*, 2008, **2008**, pdb.prot4986.
34. Chen, J. *et al.*, Multiphoton microscopic imaging of histological sections without hematoxylin and eosin staining differentiates carcinoma *in situ* lesion from normal oesophagus. *Appl. Phys. Lett.*, 2013, **103**, 18.
35. Gibbs, S. L. *et al.*, Near-infrared fluorescent digital pathology for the automation of disease diagnosis and biomarker assessment. *Mol. Imaging*, 2015, **14**, 7290.2015.00005.
36. Bouma, B. (ed.), *Handbook of Optical Coherence Tomography*, CRC Press, Boca Raton, 2001.
37. Lin, S.-E. *et al.*, Rapid pseudo-H&E imaging using a fluorescence-inbuilt optical coherence microscopic imaging system. *Biomed. Opt. Express*, 2021, **12**, 5139.
38. Liu, H. *et al.*, Single-shot semi-quantitative phase contrast microscopy. In Focus on Microscopy Conference, Oporto, Portugal, 2023.
39. Tehrani, K. F., Xu, J., Zhang, Y., Shen, P. and Kner, P., Adaptive optics stochastic optical reconstruction microscopy (AO-STORM) using a genetic algorithm. *Opt. Express*, 2015, **23**, 13677.

ACKNOWLEDGEMENTS. A.B. thanks the Department of Higher Education, Ministry of Education, Government of India, for financial support. A.K. thanks the Indian Institute of Technology Guwahati for the Institute Post-Doctoral Fellowship.

Received 19 June 2023; revised accepted 27 September 2023

doi: 10.18520/cs/v126/i2/244-254